UDSpace Institutional Repository
University of Delaware Open Access Articles

Wang, T., Ni, C., & Janotti, A. (2017). Band alignment and p-type doping of ZnSnN2. Physical Review B, 95(20).
http://dx.doi.org/10.1103/physrevb.95.205205

DOI: 10.1103/PhysRevB.95.205205

©2015 American Physical Society

This article is made available in accordance with the University of Delaware Faculty Policy on Open Access (4.2.15) and the publisher's policy.

PHYSICAL REVIEW B **95**, 205205 (2017)

Band alignment and *p*-type doping of $ZnSnN_2$

Tianshi Wang, Chaoying Ni, and Anderson Janotti
Department of Materials Science and Engineering, University of Delaware, Newark, Delaware 19716, USA

(Received 27 February 2017; published 31 May 2017)

Composed of earth-abundant elements, $ZnSnN_2$ is a promising semiconductor for photovoltaic and photoelectrochemical applications. However, basic properties such as the precise value of the band gap and the band alignment to other semiconductors are still unresolved. For instance, reported values for the band gap vary from 1.4 to 2.0 eV. In addition, doping in $ZnSnN_2$ remains largely unexplored. Using density functional theory with the Heyd-Scuseria-Ernzerhof hybrid functional, we investigate the electronic structure of $ZnSnN_2$, its band alignment to GaN and ZnO, and the possibility of *p*-type doping. We find that the position of the valence-band maximum of $ZnSnN_2$ is 0.39 eV higher than that in GaN, yet the conduction-band minimum is close to that in ZnO, which suggests that achieving *p*-type conductivity is likely as in GaN, yet it may be difficult to control unintentional *n*-type conductivity as in ZnO. Among possible *p*-type dopants, we explore Li, Na, and K substituting on the Zn site. We show that while Li_{Zn} is a shallow acceptor, Na_{Zn} and K_{Zn} are deep acceptors, which we trace back to large local relaxations around the Na and K impurities due to the atomic size mismatches.

DOI: 10.1103/PhysRevB.95.205205

I. INTRODUCTION

The nitrides Zn-IV-N_2 are promising semiconductor materials for photovoltaic and photoelectrochemical cells [1] and could also complement the group-III nitrides and their alloys in optoelectronic and electronic applications [2]. By adding Si and Ge, the direct band gaps of Zn(Si,Ge,Sn)N_2 alloys are predicted to cover all the visible-light spectrum [3–5], making them promising for full-spectrum LED applications. In contrast, InGaN alloys can hardly be used at longer wavelengths beyond the blue and green spectral regions, in part due to segregation at high indium concentrations [6–8]. In addition, in Zn-IV-N_2, Zn, Si, and Sn are earth abundant and environment friendly as opposed to the increasingly high cost of indium. The crystal structure of Zn-IV-N_2 is derived from that of wurtzite III-nitride, where the group-III ions are replaced by alternating Zn and group-IV ions, resulting in an orthorhombic structure as shown in Fig. 1(a). The local valence requirement of two electrons per bond is still fulfilled. $ZnSnN_2$ is an example of this class of ternary nitrides. It has been synthesized by different methods, including the vapor-liquid-solid method [3], reactive radio frequency magnetron sputtering deposition [9], and molecular beam epitaxy (MBE) [10]; nevertheless, $ZnSnN_2$ is still at the early stages of development [5].

The calculated band gap of $ZnSnN_2$ is direct at Γ, yet the reported values vary in a wide range, from 1.4 eV to 2.0 eV [2,5,9,11,12]. Calculations based on the Heyd-Scuseria-Ernzerhof (HSE) hybrid functional give a gap of 1.42 eV for mixing parameter $\alpha = 0.25$ (25% Hartree-Fock exchange) [9] and 1.84 eV for $\alpha = 0.31$ [2,13], while calculations based on the PBE0 hybrid functional give a gap of 2 eV [12]. Using the quasiparticle self-consistent *GW* method, Punya *et al.* [4] reported a gap of 2.15 eV using lattice parameters based on the local density approximation (LDA) and, more recently, 1.8 ± 0.1 eV [11] using experimental values for the lattice parameters. Experimental values for the band gap, based on the absorption onset or photoluminescence spectra, lie in a wider range, from 0.95 to 2.38 eV [3,9,14–17]. It has been argued that $ZnSnN_2$ samples are typically *n* type with high free carrier concentrations in the range 10^{18}–10^{21} cm^{-3} [9,14], leading to a significant Burstein-Moss shift that explains the observed larger band gap values [9], while lower band gap values are attributed to high degrees of cation disorder [5,14]. Recent experiments indicate that a wurtzite phase can be stabilized at low growth temperatures as well [18], and this could also possibly explain the observed lower band gaps.

Based on results of first-principles calculations, Chen *et al.* [13] explained that $ZnSnN_2$ is *n* type because of low formation energy of native defects that act as shallow donors, such as Sn_{Zn} antisites, and possible contamination by O_N impurities. Recent experiments corroborate this picture by finding that the carrier density can be tuned by changing the cation composition ratio [17]. As yet, *p*-type doping has not been explored. It is not clear whether $ZnSnN_2$ could be made *p* type as GaN, or whether *p*-type conductivity would be difficult to realize as in ZnO. Punya *et al.* [11] calculated band offsets between $ZnSnN_2$, GaN, and ZnO using the quasiparticle self-consistent *GW* method. They reported that the valence-band maximum (VBM) of $ZnSnN_2$ is higher than that of GaN by 1.9 eV [11]. This very large valence-band offset is difficult to explain because it represents a huge and unexpected deviation from the common anion rule [19]. For furthering the development of $ZnSnN_2$ as a semiconductor for device applications, it is essential to know a series of basic properties besides the band gap, e.g., the position of the band edges with respect to that of other semiconductors, and how to control electrical conductivity: Is it possible to achieve both *n*-type and *p*-type conductivity in $ZnSnN_2$?

Here we use density functional calculations based on the HSE hybrid functional to determine the electronic band structure of $ZnSnN_2$ and the band offsets between $ZnSnN_2$ and two common wide-band-gap semiconductors, wurtzite GaN and ZnO. We also explore the possibility of *p*-type doping in $ZnSnN_2$. In the following, we first describe the details of the calculations, and present the results for the electronic band structure; then we discuss the results for the band alignment, and finally we address *p*-type doping, exploring alkali metals Li, Na, and K substituting on the Zn site as possible shallow acceptors.

©2017 American Physical Society

II. COMPUTATIONAL METHODS

Our calculations are based on the density functional theory (DFT) [20,21] and the screened hybrid functional of Heyd-Scuseria-Ernzerhof (HSE) [22] as implemented in the VASP code [23,24]. In the HSE approach, the exchange potential is separated into short-range and long-range parts, and the nonlocal Hartree-Fock exchange is mixed with the generalized gradient approximation (GGA) exchange [25] only in the short-range part. The fraction of Hartree-Fock exchange is represented by a mixing parameter α, with a typical value of 0.25. The HSE functional has been shown to produce accurate band gaps for many semiconductors [26,27], in contrast to the LDA or the GGA which severely underestimate band gaps [28]. However, in the case of GaN and ZnO, α must be increased to 0.31 and 0.38 for a correct description of band gaps, band alignments, and defect levels [29–31]. A test using the *GW* within the G_0W_0 approximation, as implemented in the VASP code, on top of the HSE calculation with $\alpha = 0.25$ gives a correction of only 0.1 eV to the quasiparticle band gap compared to that of HSE with $\alpha = 0.31$. Therefore, we use HSE with $\alpha = 0.31$, as in GaN, for the band structure and impurity calculations in $\mathrm{ZnSnN_2}$.

Projector augmented wave (PAW) potentials are used to describe the interaction between the valence electrons and the frozen ion cores [32]. The PAW potentials for Zn, Sn, and N contain 12, 4, and 5 valence electrons, respectively, i.e., Zn: $3d^{10}4s^2$, Sn: $5s^25p^2$, N: $2s^23p^3$. For obtaining the equilibrium lattice parameters of $\mathrm{ZnSnN_2}$, we used the orthorhombic cell with 16 atoms shown in Fig. 1(a), with a $4 \times 4 \times 4$ mesh of k points for integrations over the Brillouin zone. For GaN and ZnO, we used the primitive wurtzite cell with 4 atoms, with a $6 \times 6 \times 4$ mesh of k points. We use a cutoff of 500 eV for the plane wave basis set in all calculations.

The formation enthalpy of $\mathrm{ZnSnN_2}$ is given by

$$\Delta H^f(\mathrm{ZnSnN_2}) = E_{\mathrm{tot}}(\mathrm{ZnSnN_2}) - E_{\mathrm{tot}}(\mathrm{Zn}) - E_{\mathrm{tot}}(\mathrm{Sn}) - E_{\mathrm{tot}}(\mathrm{N_2}), \qquad (1)$$

where $E_{\mathrm{tot}}(\mathrm{ZnSnN_2})$ is the total energy per formula unit of $\mathrm{ZnSnN_2}$, $E_{\mathrm{tot}}(\mathrm{Zn})$ and $E_{\mathrm{tot}}(\mathrm{Sn})$ are the total energies of bulk Zn in hexagonal-close-packed structure and Sn in the diamond crystal structure. The last term, $E_{\mathrm{tot}}(\mathrm{N_2})$, is the total energy of an isolated $\mathrm{N_2}$ molecule.

The band alignment between $\mathrm{ZnSnN_2}$ and GaN (ZnO) is calculated using a standard procedure as described elsewhere [33]. First, the VBM of $\mathrm{ZnSnN_2}$ and GaN (ZnO) are determined with respect to the averaged electrostatic potential in bulk calculations. Then, the averaged electrostatic potentials are aligned by performing an interface calculation. In this case, we used a supercell composed of 12 layers of each material with two equivalent interfaces, in a superlattice configuration as shown in Fig. 1(b). We chose a superlattice along the nonpolar [100] direction of the $\mathrm{ZnSnN_2}$ orthorhombic structure and $[11\bar{2}0]$ of the GaN (ZnO) wurtzite crystal structure to avoid the directions of spontaneous polarization, and the problems resulting from the polar discontinuity. The positions of the atoms in the bulk regions of the superlattice were fixed and the positions of the atoms at the interface layers were allowed to relax. The in-plane lattice parameters were set to the average of those of $\mathrm{ZnSnN_2}$ and GaN (ZnO) and the out-of-plane dimensions were chosen such that the equilibrium volume of each material is conserved. We also have tested using the in-plane lattice parameters of GaN and of $\mathrm{ZnSnN_2}$, making sure that the volume of the strained material is equal to its equilibrium volume. The results of these tests show an error of ±0.07 eV in the averaged electrostatic potential differences. For the mixing parameter in HSE, we tested using $\alpha = 0.25$, 0.31, and 0.38 for the superlattice calculations. We find the averaged electrostatic potential differences for the three mixing parameters vary within 0.05 eV. This is expected since the averaged electrostatic potential contains only the Hartree term, and depends mostly on the volume as long as the PAW potentials and the number of electrons are kept the same.

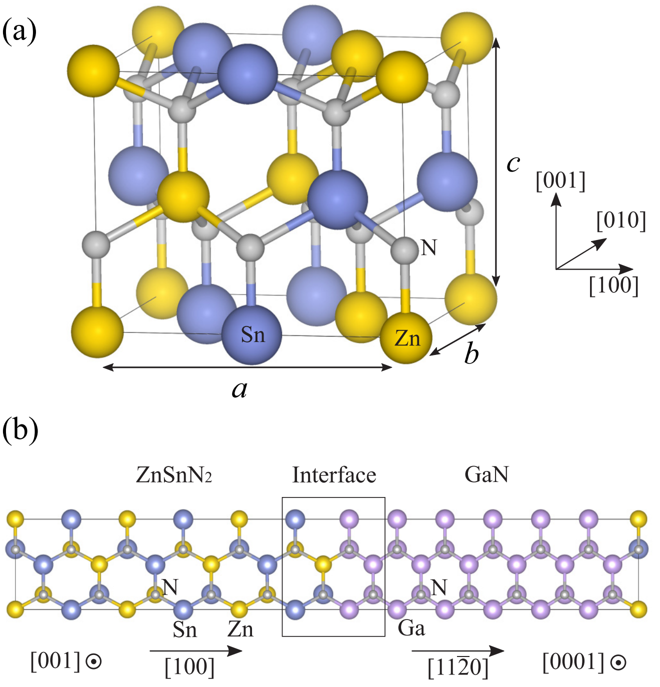

FIG. 1. (a) $\mathrm{ZnSnN_2}$ $Pna2_1$ orthorhombic structure. The lattice parameters a, b, and c are indicated. (b) Structure of the $\mathrm{ZnSnN_2/GaN}$ (ZnO) superlattice used for determining the alignment of the averaged electrostatic potential in the bulk regions of $\mathrm{ZnSnN_2}$ and GaN (ZnO).

The calculations described above are for natural band offsets, i.e., the relative position of the band edges of two materials, in their equilibrium structures, with respect to the vacuum level. We have also considered a pseudomorphic interface where the in-plane lattice parameters are those of GaN and the out-of-plane lattice parameter of the heterostructure is allowed to relax, minimizing the total energy. Since the $\mathrm{ZnSnN_2}$ layer is compressed in the in-plane directions, it expands in the out-of-plane direction but does not fully recover its equilibrium volume. This is referred to strained $\mathrm{ZnSnN_2}$ case below. By comparing the natural band offset with the band offset for $\mathrm{GaN/ZnSnN_2}$ with strained $\mathrm{ZnSnN_2}$, we derive absolute deformation potentials for the valence band (a_v) and for the conduction band (a_c), and compare to the reported values for GaN and ZnO [33].

The calculations for impurities in $\mathrm{ZnSnN_2}$ are carried out using a supercell of 128 atoms, which is a $2 \times 2 \times 2$ repetition of the 16-atom unit cell, with $(\frac{1}{4},\frac{1}{4},\frac{1}{4})$ as the special k point for integrations over the Brillouin zone. As acceptor impurities, we considered Li, Na, and K substituting on the Zn site, in analogy to Mg doping in GaN. The likelihood of incorporating an impurity in a crystal is determined by its formation energy. In this case, the formation energy of a defect (e.g., $\mathrm{Li_{Zn}}$) in charge state q is defined as [31]

$$E^f(\mathrm{Li}_{\mathrm{Zn}}^q) = E_{\mathrm{tot}}(\mathrm{Li}_{\mathrm{Zn}}^q) - E_{\mathrm{tot}}(\mathrm{ZnSnN_2}) + E_{\mathrm{tot}}(\mathrm{Zn}) + \mu_{\mathrm{Zn}} - E_{\mathrm{tot}}(\mathrm{Li}) - \mu_{\mathrm{Li}} + q(\varepsilon_F + E_v) + \Delta^q, \tag{2}$$

where $E_{\mathrm{tot}}(\mathrm{Li}_{\mathrm{Zn}}^q)$ is the total energy of the supercell containing one Li sitting on a Zn site in charge state q, and $E_{\mathrm{tot}}(\mathrm{ZnSnN_2})$ is the total energy of a perfect $\mathrm{ZnSnN_2}$ crystal in the same supercell. The chemical potential of Li (μ_{Li}) is referenced to the total energy per atom of Li bulk [$E_{\mathrm{tot}}(\mathrm{Li})$], whereas μ_{Zn} is referenced to the total energy per atom of Zn bulk [$E_{\mathrm{tot}}(\mathrm{Zn})$]. The energy of the electron reservoir is the Fermi level ε_F, referenced to the valence-band maximum E_v of bulk $\mathrm{ZnSnN_2}$. Finally, Δ^q is the correction due to the finite size of the supercell [34].

III. RESULTS AND DISCUSSION

A. Crystal structure and electronic structure

The calculated lattice parameters of $\mathrm{ZnSnN_2}$, GaN, and ZnO are listed in Table I. The results are in good agreement with previous calculations [13,30,35] and experimental data [3,36,37]. The calculated formation enthalpy of $\mathrm{ZnSnN_2}$ is −0.23 eV, in agreement with the value of −0.17 eV from previous calculations [13]. The small formation enthalpy indicates that the synthesis of high-quality $\mathrm{ZnSnN_2}$ using the stable phase of the composing elements can be quite challenging [5].

The electronic band structure of $\mathrm{ZnSnN_2}$ is shown in Fig. 2(a). $\mathrm{ZnSnN_2}$ has a direct band gap at the Γ point. The calculated band gap using the HSE functional depends on the mixing parameter α. For $\alpha = 0.31$, we obtain a gap of 1.75 eV, in good agreement with previous calculations [13]. Room-temperature photoluminescence excitation spectroscopy measurements give a value of 1.7 ± 0.1 eV [3]. For comparison, GGA ($\alpha = 0$) severely underestimates the band gap, resulting in a gap of only 0.1 eV. Compared to the GGA

TABLE I. Calculated equilibrium lattice parameters for $\mathrm{ZnSnN_2}$, GaN, and ZnO using the HSE hybrid functional with mixing parameters $\alpha = 0$ (GGA), 0.25, 0.31, and 0.38. For comparison, the experimental values are also listed: for GaN from Ref. [36], for ZnO from Ref. [37], and for $\mathrm{ZnSnN_2}$ from Ref. [3].

		GGA	$\alpha = 0.25$	$\alpha = 0.31$	$\alpha = 0.38$	Exp.
GaN	a (Å)	3.247	3.201	3.192	3.181	3.19
	c (Å)	5.281	5.202	5.185	5.167	5.19
ZnO	a (Å)	3.282	3.261	3.255	3.249	3.248
	c (Å)	5.319	5.232	5.218	5.203	5.204
$\mathrm{ZnSnN_2}$	a (Å)	6.810	6.743	6.733	6.712	6.753
	b (Å)	5.912	5.855	5.839	5.827	5.842
	c (Å)	5.543	5.468	5.452	5.436	5.462

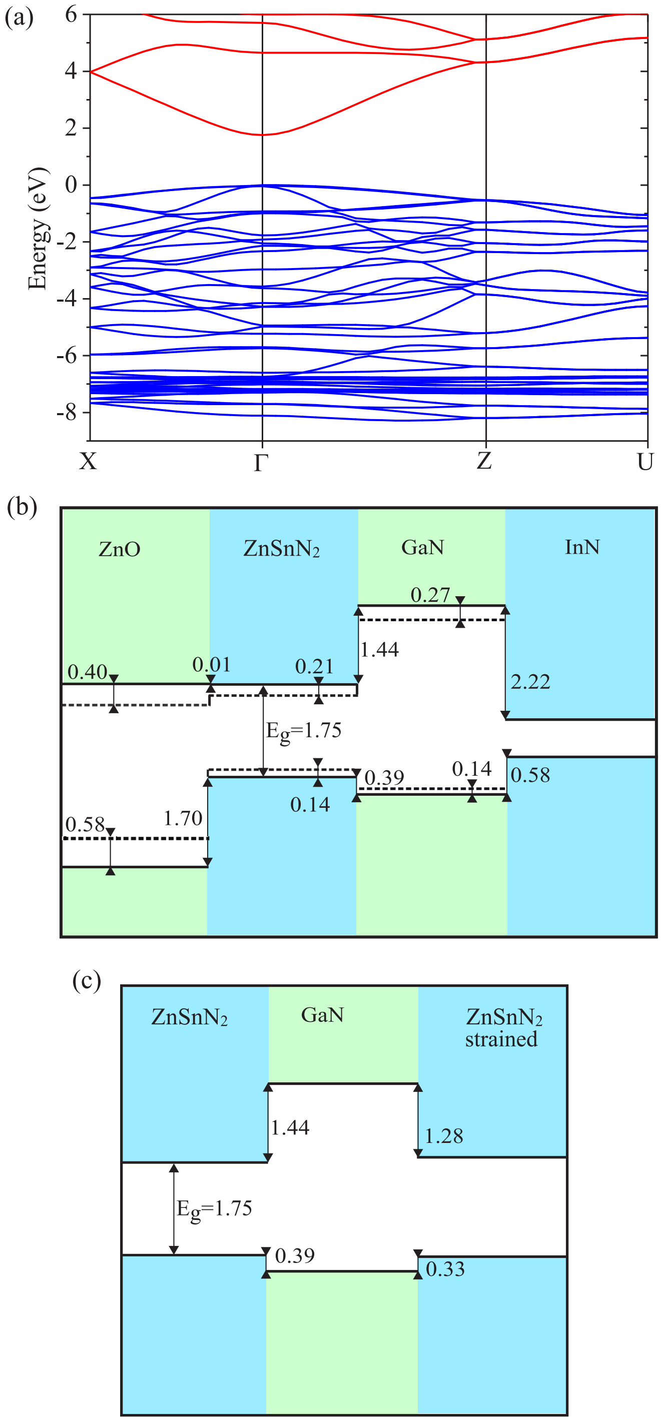

FIG. 2. (a) Calculated electronic band structure of $\mathrm{ZnSnN_2}$ using HSE with mixing parameter $\alpha = 0.31$. The zero in the energy axis corresponds to the valence-band maximum. (b) Band alignment between $\mathrm{ZnSnN_2}$ and GaN, and between $\mathrm{ZnSnN_2}$ and ZnO. These correspond to natural band offsets, i.e., the relative position of the band edges in each material, in their equilibrium lattice parameters. The experimental value for the band alignment between GaN and InN, from Ref. [38], is also included. The dashed lines correspond to results using mixing parameter $\alpha = 0.25$ in HSE. (c) Band alignment at the GaN/$\mathrm{ZnSnN_2}$ for unstrained and strained (pseudomorphic) $\mathrm{ZnSnN_2}$ cases. All values are in eV.

value with the lattice parameters fixed to those obtained using HSE with $\alpha = 0.31$, we find that HSE corrects the gap by pushing down the valence band by 0.60 eV and pushing up the conduction band by 0.90 eV. As shown in the electronic band structure of $ZnSnN_2$ [Fig. 2(a)], the relatively flat Zn 3*d* bands show up at ∼7 eV below the VBM. The conduction-band minimum (CBM), on the other hand, is derived mostly from Zn *s* orbitals.

B. Band alignments

The calculated band alignments between $ZnSnN_2$ and GaN and between $ZnSnN_2$ and ZnO are shown in Fig. 2(b). For these calculations, we used lattice parameters obtained in HSE using $\alpha = 0.31$ for $ZnSnN_2$ and GaN, and $\alpha = 0.38$ for ZnO. The VBM with respect to the averaged electrostatic in the bulk calculations was determined using $\alpha = 0.25$ and 0.31 for $ZnSnN_2$ and GaN, and $\alpha = 0.25$ and 0.38 for ZnO. Again, we note that the difference in the averaged electrostatic potentials in the interface calculations does not depend on the mixing parameter, as long as the volume of the superlattice is kept fixed.

We find that the VBM of $ZnSnN_2$ is higher than that of GaN by 0.39 eV. This can be attributed largely to the stronger repulsion between the Zn 3*d* states and the N 2*p* states in $ZnSnN_2$ than that between the Ga 3*d* and N 2*p* in GaN. Note that this result is independent of the mixing parameter α. We also find that the VBM of $ZnSnN_2$ is 1.70 eV higher than that of ZnO, and this is attributed largely to the difference in the energy position of the N 2*p* and O 2*p* orbitals. These results are in contrast to those in Ref. [11] where a valence-band offset of 1.9 eV is reported for $ZnSnN_2$ and GaN. Based on the common anion rule, one would expect the valence band offset between $ZnSnN_2$ and GaN to be much smaller, as our results indicate. Moreover, based on the transitivity rule, we obtain a valence band offset between GaN and ZnO of 1.31 eV, in good agreement with the value of 1.37 eV deduced from measurements of x-ray photoemission spectroscopy for ZnO/AlN and the established values for GaN/AlN [39]. We note, however, that our results are in disagreement with the experimental results of Liu *et al.* [40], who reported values between 0.7 and 0.9 eV for the valence band offset at the GaN/ZnO interface, and these are close to those predicted by Punya *et al.* [11] and Huda *et al.*[41], the latter using DFT+*U*. In the case of the conduction-band offset, we find that the CBM of $ZnSnN_2$ is 1.44 eV lower than that of GaN. In $ZnSnN_2$, the lowest conduction band is derived from Zn 4*s* states and is much lower in energy than that in GaN, derived from Ga 4*s* states. Based on a similar argument, we find that the CBM of $ZnSnN_2$ is only 0.01 eV lower than that in ZnO, since in both materials the lowest energy conduction band is derived mostly from the Zn 4*s* states. In all, further experiments are called for solving the discrepancies in the calculated band alignments.

For the band offset between GaN and the pseudomorphic $ZnSnN_2$ layer, where the in-plane lattice parameters are those of GaN and the out-of-plane lattice parameter of the heterostructure is allowed to relax, we find a valence-band offset of 0.33 eV and a conduction-band offset of 1.28 eV. The volume of the strained $ZnSnN_2$ is 5.64% smaller than the equilibrium volume. From the calculations of the band alignments between GaN and unstrained $ZnSnN_2$ and between GaN and strained (pseudomorphic) $ZnSnN_2$ shown in Fig. 2(c), we determined the absolute deformation potential for the valence band a_v and for the conduction band a_c. We find $a_v = 1.06$ eV and $a_c = -2.84$ eV; for the band gap deformation potential, we find $a_g = -3.90$ eV. These results are within the range of values reported for GaN and ZnO [33], since the valence-band maximum of $ZnSnN_2$ is derived from N 2*p* and the conduction-band minimum is derived from Zn 4*s* states.

Based on the calculated position of the band edges of $ZnSnN_2$ with respect to those of GaN and ZnO, we can infer the possibility of *n*-type and *p*-type doping. For instance, ZnO can be made *n* type quite easily, largely due to the low position of its CBM in an absolute energy scale [42]. Most donor impurities, including H [43], result in shallow donor levels. We therefore expect the same conclusions to hold in the case of $ZnSnN_2$. On the other hand, ZnO cannot be made *p* type by substituting Li or Na on the Zn site, since these impurities are deep acceptors. This can be attributed to the VBM in ZnO being too low with respect to the vacuum level [44]. All the acceptor impurities tested so far seem to lead to deep acceptor levels [42]. On the other hand, GaN can be made *p* type by incorporating Mg on the Ga site. Since the VBM of $ZnSnN_2$ is higher than that of GaN by 0.39 eV, one would expect that $ZnSnN_2$ could be made *p* type as GaN. Similar arguments can be used in comparison with InN, which has been shown to be *p*-type dopable. However, its low-lying conduction band poses difficulties in reducing unintentional *n*-type conductivity [45].

C. Acceptor impurities in $ZnSnN_2$

For achieving *p*-type doping in $ZnSnN_2$, one would need an impurity with one less valence electron than one of the host atoms—for example, C substituting on the N site. However, C is a deep acceptor in GaN with the acceptor level at 0.9 eV above the VBM [46], and it is likely to behave as a deep acceptor in $ZnSnN_2$ as well. Besides, C could prefer to replace Sn and be electrically inactive. Choosing a column-III element to substitute on the Sn site can be problematic as well, since these impurities could also replace Zn and act as donors. Here, as candidates for shallow acceptors in $ZnSnN_2$, we considered Li, Na, and K substituting on the Zn site. Although Li, Na, and K could also incorporate at interstitial sites and behave as donors, we expect these interstitial species to be highly mobile and, therefore, be easily removed in postgrowth annealing. An analogous strategy has been demonstrated by recent experiments on Zn-rich annealed $ZnSnN_2$ with added hydrogen [47]. The results reveal that postgrowth annealing removes hydrogen and reduces carrier density down to 4×10^{16} cm^{-3}, suggesting that H be passivating acceptors.

The formation energies of Li_{Zn}, Na_{Zn}, and K_{Zn} in $ZnSnN_2$ are shown in Fig. 3(a). We find that Li displays shallow acceptor behavior, with the hole being delocalized over the whole supercell. Therefore, we only plot the formation energy of Li_{Zn} in the negative charge state. On the other hand, we find Na_{Zn} and K_{Zn} to behave as deep acceptors, with $(0/-)$ acceptor levels at 0.30 eV and 0.68 eV above the VBM. Since the formation enthalpy of $ZnSnN_2$ is rather small (−0.23 eV), we only plotted the formation energies for the Zn-rich condition.

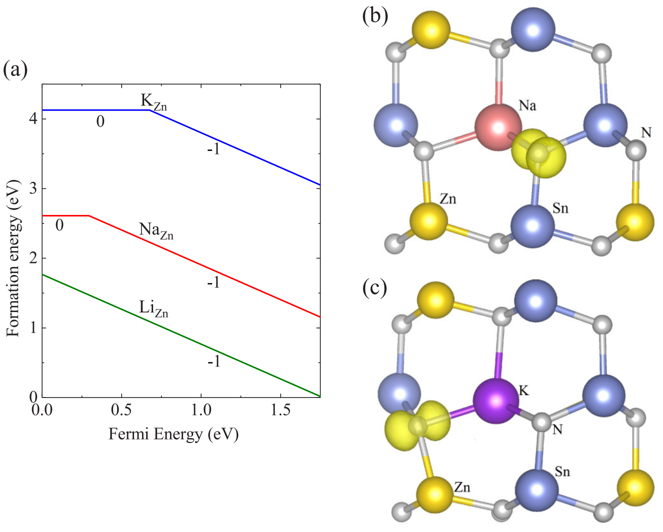

FIG. 3. (a) Formation energy of Li, Na, and K impurities in two charge states 0 and −1 as a function of the Fermi level. (b) and (c) Calculated spin density of charge-neutral Na_{Zn} and K_{Zn} in $ZnSnN_2$. The isosurface is 10% of the maximum density.

The formation energies calculated with respect to the elemental phases of Li, Na, and K show an interesting trend. They monotonically increase from Li, Na, to K. We attribute this behavior to the size mismatch between the impurity and the host Zn atom. While Li_{Zn} only slightly affects the lattice by causing small displacements of the nearest-neighbor N atoms, by 0.5% of the equilibrium bond length, Na_{Zn} and K_{Zn} cause rather large displacements, of 8.5% (Na_{Zn}) and 16.2% (K_{Zn}) of the nearest-neighbor N atoms. The displacements caused by K_{Zn} are so large that they make the neighboring N assume almost planar configurations.

The local lattice relaxations and the charge density distribution of the hole associated with neutral Na_{Zn} and K_{Zn} in $ZnSnN_2$ are shown in Figs. 3(b) and 3(c). The hole from charge-neutral Na_{Zn} or K_{Zn} becomes localized on one of the neighboring N, and in the case of K_{Zn} the N-K distance is 2.40 Å, compared to 2.07 Å for the equilibrium Zn-N bond length. Therefore, we conclude that only Li_{Zn} effectively acts as a shallow acceptor in $ZnSnN_2$, in part due to the small perturbation of the local lattice structure. However, we note that as in InN, it may be difficult to reduce the unintentional n-type conductivity in $ZnSnN_2$ due to the low-lying conduction band.

IV. SUMMARY

In conclusion, we performed hybrid functional calculations for $ZnSnN_2$ to determine its band gap and band alignment to GaN and ZnO, and to explore the possibility of p-type doping. We find that $ZnSnN_2$ has a band gap of 1.75 eV, in agreement with previous calculations and experiments. The VBM of $ZnSnN_2$ is predicted to be 0.39 eV higher than that of GaN and 1.70 eV higher than that of ZnO. The CBM of $ZnSnN_2$, on the other hand, is only 0.01 eV lower than that of ZnO. These results indicate that $ZnSnN_2$ can be made p type as GaN, and that controlling the unintentional n-type conductivity can be difficult as in ZnO. For achieving p-type conductivity, we find that Li substituting on the Zn site displays shallow acceptor behavior, whereas Na and K lead to deep levels. The deep level behaviors of Na_{Zn} and K_{Zn} are attributed to very large lattice relaxations that make the neighboring N atoms assume almost planar positions with the hole localized on one of them.

ACKNOWLEDGMENTS

T.W. and C.N. gratefully acknowledge financial support from the II-VI Foundation, and A.J. is grateful for financial support from the National Science Foundation under Grant No. 1652994. This research was supported through the use of the Extreme Science and Engineering Discovery Environment (XSEDE) supercomputer facility, National Science Foundation Grant No. ACI-1053575, and the Information Technologies (IT) resources at the University of Delaware, specifically the high-performance computing resources.

---

[1] A. Zakutayev, J. Mater. Chem. A **4**, 6742 (2016).

[2] P. Narang, S. Chen, N. C. Coronel, S. Gul, J. Yano, L. W. Wang, N. S. Lewis, and H. A. Atwater, Adv. Mater. **26**, 1235 (2014).

[3] P. C. Quayle, K. He, J. Shan, and K. Kash, MRS Commun. **3**, 135 (2013).

[4] A. Punya, W. R. L. Lambrecht, and M. van Schilfgaarde, Phys. Rev. B **84**, 165204 (2011).

[5] T. D. Veal, N. Feldberg, N. F. Quackenbush, W. M. Linhart, D. O. Scanlon, L. F. J. Piper, and S. M. Durbin, Adv. Energy Mater. **5**, 1501462 (2015).

[6] Z. Liliental-Weber, D. N. Zakharov, K. M. Yu, J. W. Ager III, W. Walukiewicz, E. E. Haller, H. Lu, and W. J. Schaff, J. Electron Microsc. **54**, 243 (2005).

[7] M. K. Horton, S. Rhode, S. L. Sahonta, M. J. Kappers, S. J. Haigh, T. J. Pennycook, C. J. Humphreys, R. O. Dusane, and M. A. Moram, Nano Lett. **15**, 923 (2015).

[8] Z. Deng, Y. Jiang, W. Wang, L. Cheng, W. Li, W. Lu, H. Jia, W. Liu, J. Zhou, and H. Chen, Sci. Rep. **4**, 6734 (2014).

[9] L. Lahourcade, N. C. Coronel, K. T. Delaney, S. K. Shukla, N. A. Spaldin, and H. A. Atwater, Adv. Mater. **25**, 2562 (2013).

[10] N. Feldberg, J. D. Aldous, P. A. Stampe, R. J. Kennedy, T. D. Veal, and S. M. Durbin, J. Electron. Mater. **43**, 884 (2014).

[11] A. Punya and W. R. L. Lambrecht, Phys. Rev. B **88**, 075302 (2013).

[12] N. Feldberg, B. Keen, J. D. Aldous, D. O. Scanlon, P. A. Stampe, R. J. Kennedy, R. J. Reeves, T. D. Veal, and S. M. Durbin, in *38th IEEE Photovoltaic Specialists Conference 2012* (IEEE, Austin, TX, 2012), pp. 2524–2527.

[13] S. Chen, P. Narang, H. A. Atwater, and L.-W. Wang, Adv. Mater. **26**, 311 (2014).

[14] N. Feldberg, J. D. Aldous, W. M. Linhart, L. J. Phillips, K. Durose, P. A. Stampe, R. J. Kennedy, D. O. Scanlon, G. Vardar,

R. L. Field, T. Y. Jen, R. S. Goldman, T. D. Veal, and S. M. Durbin, Appl. Phys. Lett. **103**, 042109 (2013).
[15] P. C. Quayle, E. W. Blanton, A. Punya, G. T. Junno, K. He, L. Han, H. Zhao, J. Shan, W. R. L. Lambrecht, and K. Kash, Phys. Rev. B **91**, 205207 (2015).
[16] F. Deng, H. Cao, L. Liang, J. Li, J. Gao, and H. Zhang, Opt. Lett. **40**, 1282 (2015).
[17] A. N. Fioretti, A. Zakutayev, H. Moutinho, C. Melamed, J. D. Perkins, A. G. Norman, M. Al-Jassim, E. S. Toberer, and A. C. Tamboli, J. Mater. Chem. C **3**, 11017 (2015).
[18] N. Senabulya, N. Feldberg, R. A. Makin, Y. Yang, G. Shi, C. M. Jones, E. Kioupakis, J. Mathis, R. Clarke, and S. M. Durbin, AIP Adv. **6**, 075019 (2016).
[19] J. O. McCaldin, T. C. McGill, and C. A. Mead, Phys. Rev. Lett. **36**, 56 (1976).
[20] P. Hohenberg and W. Kohn, Phys. Rev. **136**, B864 (1964).
[21] W. Kohn and L. J. Sham, Phys. Rev. **140**, A1133 (1965).
[22] J. Heyd, G. E. Scuseria, and M. Ernzerhof, J. Chem. Phys. **118**, 8207 (2003).
[23] G. Kresse and J. Hafner, Phys. Rev. B **47**, 558 (1993).
[24] G. Kresse and J. Hafner, Phys. Rev. B **49**, 14251 (1994).
[25] J. P. Perdew, K. Burke, and M. Ernzerhof, Phys. Rev. Lett. **77**, 3865 (1996).
[26] J. Heyd and G. E. Scuseria, J. Chem. Phys. **121**, 1187 (2004).
[27] J. Paier, M. Marsman, K. Hummer, G. Kresse, I. C. Gerber, and J. G. Angyán, J. Chem. Phys. **124**, 154709 (2006).
[28] R. W. Godby, M. Schlüter, and L. J. Sham, Phys. Rev. B **37**, 10159 (1988).
[29] F. Oba, A. Togo, I. Tanaka, J. Paier, and G. Kresse, Phys. Rev. B **77**, 245202 (2008).
[30] J. L. Lyons, A. Janotti, and C. G. Van de Walle, Phys. Rev. B **89**, 035204 (2014).
[31] C. Freysoldt, B. Grabowski, T. Hickel, J. Neugebauer, G. Kresse, A. Janotti, and C. G. Van de Walle, Rev. Mod. Phys. **86**, 253 (2014).
[32] P. E. Blöchl, Phys. Rev. B **50**, 17953 (1994).
[33] A. Janotti and C. G. Van de Walle, Phys. Rev. B **75**, 121201 (2007).
[34] C. Freysoldt, J. Neugebauer, and C. G. Van de Walle, Phys. Status Solidi **248**, 1067 (2011).
[35] M. Debbichi, T. Sakhraoui, L. Debbichi, and M. Said, J. Alloys Compd. **578**, 602 (2013).
[36] O. Lagerstedt and B. Monemar, Phys. Rev. B **19**, 3064 (1979).
[37] R. R. Reeber, J. Appl. Phys. **41**, 5063 (1970).
[38] P. D. C. King, T. D. Veal, C. E. Kendrick, L. R. Bailey, S. M. Durbin, and C. F. McConville, Phys. Rev. B **78**, 033308 (2008).
[39] T. D. Veal, P. D. C. King, S. A. Hatfield, L. R. Bailey, C. F. McConville, B. Martel, J. C. Moreno, E. Frayssinet, F. Semond, and J. Zúñiga-Pérez, Appl. Phys. Lett. **93**, 202108 (2008).
[40] J. W. Liu, A. Kobayashi, S. Toyoda, H. Kamada, A. Kikuchi, J. Ohta, H. Fujioka, H. Kumigashira, and M. Oshima, Phys. Status Solidi **248**, 956 (2011).
[41] M. N. Huda, Y. Yan, S.-H. Wei, and M. M. Al-Jassim, Phys. Rev. B **78**, 195204 (2008).
[42] A. Janotti and C. G. Van de Walle, Rep. Prog. Phys. **72**, 126501 (2009).
[43] A. Janotti and C. G. Van de Walle, Nat. Mater. **6**, 44 (2007).
[44] J. L. Lyons, A. Janotti, and C. G. Van de Walle, J. Appl. Phys. **115**, 012014 (2014).
[45] J. W. Ager, R. E. Jones, D. M. Yamaguchi, K. M. Yu, W. Walukiewicz, S. X. Li, E. E. Haller, H. Lu, and W. J. Schaff, Phys. Status Solidi **244**, 1820 (2007).
[46] J. L. Lyons, A. Janotti, and C. G. Van de Walle, Appl. Phys. Lett. **97**, 152108 (2010).
[47] A. N. Fioretti, A. Stokes, M. R. Young, B. Gorman, E. S. Toberer, A. C. Tamboli, and A. Zakutayev, Adv. Electron. Mater. **3**, 1600544 (2017).